arXiv:0903.3476v1 [cond-mat.stat-mech] 20 Mar 2009

Fractality of the non-equilibrium stationary states of open volume-preserving systems: I. Tagged particle diffusion

Felipe Barra,[1] Pierre Gaspard,[2] and Thomas Gilbert[2]

[1]*Departamento de Física, Facultad de Ciencias Físicas y Matemáticas, Universidad de Chile, Casilla 487-3, Santiago Chile*

[2]*Center for Nonlinear Phenomena and Complex Systems, Université Libre de Bruxelles, C. P. 231, Campus Plaine, B-1050 Brussels, Belgium*

(Dated: March 20, 2009)

Deterministic diffusive systems such as the periodic Lorentz gas, multi-baker map, as well as spatially periodic systems of interacting particles, have non-equilibrium stationary states with fractal properties when put in contact with particle reservoirs at their boundaries. We study the macroscopic limits of these systems and establish a correspondence between the thermodynamics of the macroscopic diffusion process and the fractality of the stationary states that characterize the phase-space statistics. In particular the entropy production rate is recovered from first principles using a formalism due to Gaspard [J. Stat. Phys. **88**, 1215 (1997)]. This article is the first of two; the second article considers the influence of a uniform external field on such systems.

PACS numbers: 05.45.-a,05.70.Ln,05.60.-k

I. INTRODUCTION

The assumption that the microscopic dynamics of mechanical systems obeying Newton's equations are mixing offers a mechanism by which the entropy can increase toward its equilibrium value, as described by Gibbs in 1902 [1]. The mixing would indeed allow coarse-grained probabilities to reach their equilibrium values after a long time, a result that has received a rigorous meaning in the context of modern ergodic theory [2]. The use of the coarse-grained entropy of a physical system, which is the second ingredient of Gibbs' mechanism, is justified by the fact that, if the entropy should be given according to Boltzmann by the logarithm of the number of complexions of a system, then the introduction of cells of non-vanishing sizes is required to perform the counting of complexions in systems described by continuous coordinates.

The program set up by Gibbs has taken on a new perspective in recent years with its systematic application to chaotic, deterministic volume-preserving dynamical systems sustaining a transport process of diffusion, which therefore fall under the scope of Liouville's theorem [3, 4, 5, 6, 7, 8, 9]. In previous works, both non-equilibrium stationary states and relaxation to equilibrium were considered, with the common thread that transport processes are intimately connected to singularities of the non-equilibrium measures, characterized by phase-space distributions with fractal properties.

A specific example of the systems of interest is the periodic Lorentz gas, in which moving particles diffuse through a lattice interacting only with fixed scatterers. A useful simplification of this process is the multi-baker map, which is a simple model of deterministic diffusion for a tracer particle with chaotic dynamics. Other higher dimensional examples are spatially periodic extensions of systems with many interacting particles, where the motion of a tagged particle is followed as it undergoes diffusion among the cells.

In refs. [8, 9], these models were studied in the context of relaxation to equilibrium. It was shown in these papers that the initial non-equilibrium distribution function rapidly develops a fractal structure in phase space due to the chaotic nature of the dynamics. This stucture is such that variations of the distribution function on arbitrarily fine scales grow as the system evolves in time. The final stages of the approach to equilibrium are then controlled by the decay of fractal, microscopic hydrodynamic modes of the system –in this case diffusive modes– which decay with time as $\exp(-\mathcal{D}k^2t)$, where k is a wave number associated to the macroscopic hydrodynamic decay, $\mathcal{D}$ is the diffusion coefficient, and t is the time. It is possible to express the rate of entropy production in this final stage in terms of measures which are determined by the non-equilibrium phase-space distribution, specified by the fractal hydrodynamic modes. The main result is that one obtains by this method exactly the expression for the rate of entropy production as given by irreversible thermodynamics for these systems [10]. The source of this agreement can be traced to the role played by the fractal hydrodynamic modes, both for requiring a coarse graining of the phase space to properly incorporate the effects of their fractal properties on entropy production in the system, as well as for describing the slowest decay of the system as it relaxes to equilibrium.

The purpose of this paper is to consider in further details the non-equilibrium stationary states of multi-baker maps and Lorentz gases which occur when their boundaries are put in contact with particle reservoirs, as well as to extend these considerations to tagged particle diffusion in spatially periodic systems of interacting particles. In the macroscopic limit, we establish the connections between the statistics of these deterministic systems and the phenomenological prescriptions of thermodynamic. Though the stationary states of multi-baker maps and Lorentz gases have been considered in some details, see

especially [11], the problem of computing the entropy production associated to the non-equilibrium stationary state has thus far been limited to the example of the multi-baker map [4]. Here we emphasize the similarities between the stationary states of multi-baker maps, Lorentz gases, and spatially periodic many particle systems, undergoing steady mass flows and show how the formalism described in [9] yields an *ab initio* derivation of the entropy production rate in all these systems.

This paper is the first of two. In the second paper [12], we will consider the Galton board [13, 14], which is to be understood in this context as a periodic finite horizon Lorentz gas with a uniform external field and no dissipation mechanism. As was recently proved by Chernov and Dolgopyat [15, 16], this system is recurrent and therefore has no drift. We will show how one can characterize equilibrium and non-equilibrium stationary states of such a system, much in the same way as with the periodic Lorentz gas we consider in this paper.

The plan of the paper is as follows. In Sec. II, we review the phenomenology of non-equilibrium diffusive systems and their entropy production. Then, starting from the Liouvillian evolution of phase-space distributions, we construct the non-equilibrium stationary states of open periodic Lorentz gases in Sec. III, as well as of multi-baker maps in Sec. IV, and show how such stationary states naturally separate between regular and singular parts. While the regular parts have the form of a local equilibrium and allow, in the continuum limit, to retrieve the phenomenological solution of a diffusive system undergoing a mass flow, the singular parts have no macroscopic counterpart and encode the dynamical details of the systems' diffusive properties. In Sec. V, these results are extended to systems of many interacting particles with non-equilibrium flux boundary conditions. Under the assumption that the dynamics of these systems is chaotic, their stationary states are shown to have properties similar to those of multi-baker maps and Lorentz gases. The singular part of the stationary states is at the origin of the entropy production rate, as is explained in Sec. VI, where the phenomenological entropy production rate is retrieved from *ab initio* considerations. Conclusions are drawn in Sec. VII.

II. PHENOMENOLOGY

The thermodynamics of deterministic models of diffusion such as the Lorentz gas and multi-baker map to be discussed below was extensively reviewed by Gaspard *et. al* in [17]. In these models, independent tracer particles mimic matter exchange processes of binary mixtures, *i.e.* the process of mutual diffusion between the light tracer particles and the infinitely heavy particles that constitute the background.

In such systems, the irreversible production of entropy arises from gradients in the density of tracer particles. For a dilute system, the resulting thermodynamic force is

$$\vec{\mathcal{X}}(\vec{X},t) = -\frac{\vec{\nabla}\mathcal{P}(\vec{X},t)}{\mathcal{P}(\vec{X},t)}\,, \tag{1}$$

where $\mathcal{P}(\vec{X},t)$ denotes the density of tracer particles at position $\vec{X}$ and time t. Here the Boltzmann constant is set to unity. Close to equilibrium, in the linear range of irreversible processes, the corresponding current is proportional to the thermodynamic force and given by Fick's law of diffusion according to

$$\vec{\mathcal{J}}(\vec{X},t) = -\mathcal{D}\vec{\nabla}\mathcal{P}(\vec{X},t)\,, \tag{2}$$

where $\mathcal{D}$ is the coefficient of diffusion of tracer particles (assumed to be uniform). In this limit, the condition of mass conservation, $\partial_t\mathcal{P}(\vec{X},t)+\vec{\nabla}\cdot\vec{\mathcal{J}}(\vec{X},t)=0$, transposes into the the Fokker-Planck equation,

$$\partial_t\mathcal{P}(\vec{X},t) = \mathcal{D}\nabla^2\mathcal{P}(\vec{X},t)\,. \tag{3}$$

The product of the thermodynamic force and current yields the rate of local irreversible production of entropy,

$$\begin{aligned}\frac{d_{\rm i}\mathcal{S}(\vec{X},t)}{dt} &= \vec{\mathcal{J}}(\vec{X},t)\cdot\vec{\mathcal{X}}(\vec{X},t)\,,\\ &= \mathcal{D}\frac{[\vec{\nabla}\mathcal{P}(\vec{X},t)]^2}{\mathcal{P}(\vec{X},t)} > 0\,.\end{aligned} \tag{4}$$

Our goal in the next sections will be to analyze the statistics of deterministic models of diffusion, identify the conditions under which their statistical evolution reduces to the evolution of macroscopic densities as described by Eq. (3) and analyze the microscopic origins of the production of entropy prescribed according to Eq. (4), which manifest themselves in the fractality of the stationary states of these models.

III. OPEN PERIODIC LORENTZ GAS

In this section, we consider a two-dimensional finite horizon periodic Lorentz gas with hexagonal symmetry, in the shape of a cylindrical Lorentz channel of length L, with periodic boundary conditions in the y-direction and absorbing boundaries at $x=\pm L/2$. Though some of the results presented in this section are original, for the most part this material is a review of existing results that can be found in Ref. [11] and references therein.

The geometry of the channel is displayed in Fig. 1 with a typical trajectory. The channel consists of a cylinder of length $L=Nl$ and height $\sqrt{3}l$ with disks $\mathbb{D}_n$, $-N\le n\le N$, of radii σ, $\sqrt{3}/4<\sigma/l<1/2$. Assuming N even, the disks' centers take positions

$$(x_n,y_n) = \begin{cases}(nl/2,0)\,, & n\,\text{odd},\\ (nl/2,\pm\sqrt{3}l/2)\,, & n\,\text{even},\end{cases} \tag{5}$$

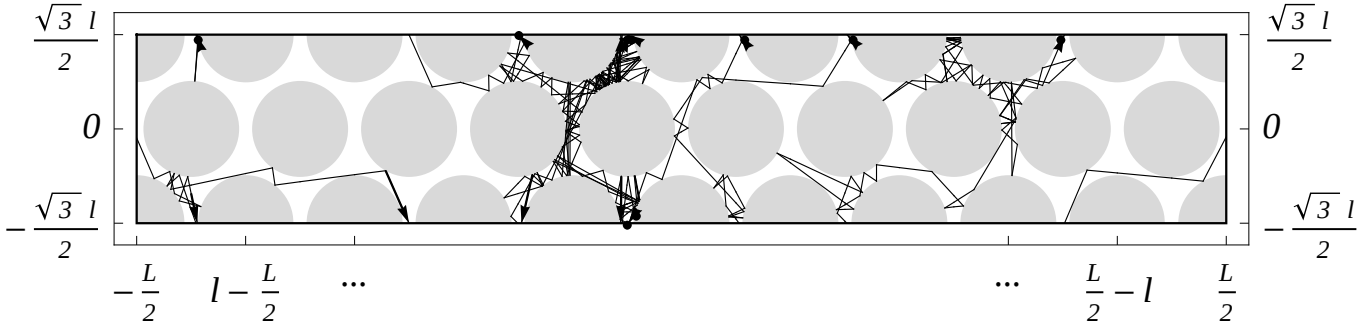

FIG. 1: Cylindrical Lorentz channel with periodic boundary conditions at the upper and lower borders. The length of the channel is L, with N identical cells of widths l and heights $\sqrt{3}l/2$, $Nl \equiv L$, each containing two disks. The disks have radii $\sigma = 0.44l$, and are positioned at points $(x, y) = (nl/2, 0)$, $n = -N+1, -N+3, \ldots, N-1$, and $(nl/2, \pm\sqrt{3}l/2)$, $n = -N, -N+2, \ldots, N-2, N$. The trajectory displayed is that of a particle which initially starts at unit velocity from the left-hand boundary, and is eventually absorbed as it reaches the right-hand boundary. Arrows on the upper and lower borders indicate points where the trajectory winds around the cylinder.

where the disks at $y = \pm\sqrt{3}l/2$ are identified. We will also denote by $\mathbb{I}_n$ the cylinder region around each disk $\mathbb{D}_n$,

$$\mathbb{I}_n = \big\{(x, y) \mid (n - 1/2)l/2 \le x \le (n + 1/2)l/2\big\}. \quad (6)$$

Thus the interior of the cylinder, where particles propagate freely is made up of the union $\cup_{n=-N}^{N} \mathbb{I}_n \setminus \mathbb{D}_n$.

The associated phase space, defined on a constant energy shell, is $\mathbb{C} = \cup_{n=-N}^{N} \mathbb{C}_n$, where $\mathbb{C}_n = \mathbb{S}^1 \otimes [\mathbb{I}_n \setminus \mathbb{D}_n]$ and the unit circle $\mathbb{S}^1$ represents all the possible velocity directions. Particles are reflected with elastic collision rules on the border $\partial\mathbb{C}$, except at the external borders, corresponding to $x = \pm L/2$, where they get absorbed. Points in phase space are denoted by Γ, $\Gamma = (x, y, v_x, v_y)$, with fixed energy $E \equiv (v_x^2 + v_y^2)/2$, and trajectories by $\Phi^t\Gamma$, with Φ^t the flow associated to the dynamics of the Lorentz channel.

The collision map takes the point $\Gamma = (x, y, v_x, v_y) \in \partial\mathbb{C}$ to $\Phi^\tau\Gamma = (x', y', v_x', v_y') \in \partial\mathbb{C}$, where τ is the time that separates the two successive collisions with the border of the Lorentz channel $\partial\mathbb{C}$, and (v_x', v_y') is obtained from (v_x, v_y) by the usual rules of specular collisions. Given that the energy E is fixed, the collision map operates on a two-dimensional surface, which, given that the collision takes place on disk n, is conveniently parameterized by the Birkhoff coordinates (ϕ_n, ξ_n), where ϕ_n specifies the angle along the border of disk n that the trajectory makes at collision with it, and ξ_n is the sinus of the angle that the particle velocity makes with respect to the outgoing normal to the disk after the collision.

A. Non-Equilibrium Stationary State

In order to set up a non-trivial stationary state, we assume that a flux of trajectories is continuously flowing through the boundaries. This can be achieved by putting the boundaries in contact with particle reservoirs such that the phase-space density at $x = \pm L/2$ is fixed according to constant values,

$$\rho(\Gamma, t)\Big|_{x=\pm L/2} = \rho_\pm, \quad (7)$$

corresponding to particle injection rates from the two ends of the channel at $x = \pm L/2$. All the injected particles have the same energy $E = (v_x^2 + v_y^2)/2$ and uniform distributions of velocity angles. The evolution of the phase-space density ρ is otherwise specified by Liouville's equation, or, equivalently, by the action of the Frobenius-Perron operator, $\widehat{P}^t$, determined according to

$$\rho(\Gamma, t) = \widehat{P}^t\rho(\Gamma, 0) \equiv \int_{\mathbb{C}} d\Gamma' \delta(\Gamma - \Phi^t\Gamma')\rho(\Gamma', 0)\,. \quad (8)$$

A remarkable result [18] is that the invariant solution of this equation, compatible with the boundary conditions (7), is given, for almost every phase point Γ, by

$$\begin{aligned}\rho(\Gamma) &= \frac{\rho_+ + \rho_-}{2} + \frac{\rho_+ - \rho_-}{L}\left[x(\Gamma) + \int_0^{-T(\Gamma)} dt\, \dot{x}(\Phi^t\Gamma)\right], \\ &= \frac{\rho_+ + \rho_-}{2} + \frac{\rho_+ - \rho_-}{L}\left\{x(\Gamma) + \sum_{k=1}^{K(\Gamma)} [x(\Phi^{-t_k}\Gamma) - x(\Phi^{-t_{k-1}}\Gamma)]\right\}. \end{aligned} \quad (9)$$

In these expressions, $x(\Gamma)$ denotes the projection of the phase point Γ on the horizontal axis, and $T(\Gamma)$ is the time it takes the phase point Γ to reach the system boundary backward in time, *i.e.* such that $x(\Phi^{-T(\Gamma)}\Gamma) = \pm L/2$. As written in the second line, the time $T(\Gamma)$ elapses in $K(\Gamma)$ successive collisions separated by time intervals τ_n, such that t_k is the time elapsed after k collision events, *viz.* $\sum_{j=1}^{k} \tau_j = t_k$. Obviously $t_{K(\Gamma)} = T(\Gamma)$. The difference $x(\Phi^{-t_k}\Gamma) - x(\Phi^{-t_{k-1}}\Gamma)$ is the displacement along the x axis between two successive collisions.

In the limit of infinite number of cells N, the number of collisions for the trajectory to reach the boundaries becomes infinite so that the invariant density can be written

$$\rho(\Gamma) \;=\; \frac{\rho_+ + \rho_-}{2} + \frac{\rho_+ - \rho_-}{L} \left\{ x(\Gamma) + \sum_{k=1}^{\infty} [x(\Phi^{-t_k}\Gamma) - x(\Phi^{-t_{k-1}}\Gamma)] \right\} . \tag{10}$$

The two contributions to this expression represent the mean linear density profile along the axis, plus fluctuations. Notice that the linear profile is itself the sum of two contributions, the first one being the equilibrium density and the second one a gradient term. These stationary states are known after Lebowitz and MacLennan [19, 20]. As noted in [18], the fluctuations form the singular part of the invariant density, which builds up according to which of the two boundaries the phase point is mapped to.

B. Continuum Limit

The linear part of the invariant density profile (9) has its origin in the diffusion process which takes place at the phenomenological level. Indeed, in the continuum limit, the phase-space density reduces to the macroscopic density distribution $\mathcal{P}(X,t)$, whose evolution is described by Eq. (3), with macroscopic position variable X and diffusion coefficient, $\mathcal{D}$, which can, in principle, be determined from the underlying dynamics.

In order to obtain Eq. (3) from the Liouvillian evolution, Eq. (8), we let $l \to 0$ and $N \to \infty$ with $Nl = L$ fixed. All other quantities are fixed, in particular the particle velocity, which is taken to be unity in the length units of L. In that limit, the macroscopic density can be obtained from the phase-space density by averaging over phase-space regions such that the position variables $x(\Gamma)$ are identified with the macroscopic position variable X, here denoted X_n and identified with the cell $\mathbb{C}_n$,

$$\mathcal{P}(X_n,t) = \frac{1}{l} \int_{\mathbb{C}_n} d\Gamma \rho(\Gamma,t) \, . \tag{11}$$

Note that the volume element is here and throughout assumed to be properly normalized, *i.e.* $\int_{\mathbb{C}_n} d\Gamma = l$.

Given non-equilibrium flux boundary conditions with the stationary state (10), the only contribution to the particle density $\mathcal{P}(X_n)$ is the linear part, which, in the continuum limit, yields the stationary solution to Eq. (3), namely

$$\mathcal{P}(X) = \frac{\mathcal{P}_+ + \mathcal{P}_-}{2} + \frac{X}{L}(\mathcal{P}_+ - \mathcal{P}_-) \, , \tag{12}$$

where $\mathcal{P}_\pm$ is equal to $\rho_\pm$ up to a volume factor, and specifies the boundary conditions $\mathcal{P}(\pm L/2)$.

The singular part of the invariant density, on the other hand, has no macroscopic counterpart. Its integration over the cell indeed vanishes by isotropy of the underlying dynamics. Nonetheless, as we will demonstrate shortly, it bears essential information pertaining to the microscopic origin of entropy production.

In that respect, the phenomenological entropy production rate (4) can be written

$$\begin{aligned} \frac{d_{\rm i}\mathcal{S}(X)}{dt} \;&=\; \mathcal{D}\frac{[\partial_X \mathcal{P}(X)]^2}{\mathcal{P}(X)}, \\ &=\; \frac{\mathcal{D}}{L^2}\frac{(\mathcal{P}_+ - \mathcal{P}_-)^2}{\mathcal{P}_{\rm eq} + \frac{X}{L}(\mathcal{P}_+ - \mathcal{P}_-)} \, , \end{aligned} \tag{13}$$

where we denoted $\mathcal{P}_{\rm eq} = (\mathcal{P}_+ + \mathcal{P}_-)/2$.

C. Numerical Results

We can verify numerically that the invariant density of the Lorentz channel has the form (9), with a linear part given by the stationary solution of the Fokker-Planck equation (12), and a singular fluctuating part. For the sake of the numerical computation, we let $L \equiv 1$ and consider a channel with $2N+1$ disks, $N = 25$, the left- and right-most ones being only half disks. The macroscopic position X, $-L/2 \le X \le L/2$, will be identified with the cells $\mathbb{C}_n$ about the corresponding disks, letting $X_n = nl/2$, $-N \le n \le N$. We then fix the injection rates $\rho_\pm$ and let $\rho_- > 0$ and $\rho_+ = 0$ so as to have $\mathcal{P}_- = 1$ and $\mathcal{P}_+ = 0$ for the corresponding macroscopic quantities.

Having fixed the geometry of the channel and the injection rates, we compute the invariant phase-space density $\rho(\Gamma)$ in terms of the corresponding density of the collision map, also called the Birkhoff map, which takes trajectories from one collision event with a disk to the next one. This is indeed much easier since the numerical integration of the Lorentz gas relies on an event driven algorithm corresponding to integrating the collision map. The conversion between the two phase-space densities is here trivial because the time scales are uniform.

Thus the linear part of the invariant density is computed by considering a large set of initial conditions injected into the channel from the left end and integrating them until they reach either ends of the channel, thus exiting the system. In the meantime, we record the number of collisions each particle performs with each disk, the ensemble average of which approximates the stationary distribution $\mathcal{P}(X_n)$. Provided N is sufficiently large and n is not too close to the channel boundaries, this ensemble average is expected to approximate $\mathcal{P}(X)$, as specified by Eq. (12). The result is displayed in Fig. 2 and was adjusted by an overall constant so as to match $\mathcal{P}_- = 1$ (and $\mathcal{P}_+ = 0$). The agreement is very good.

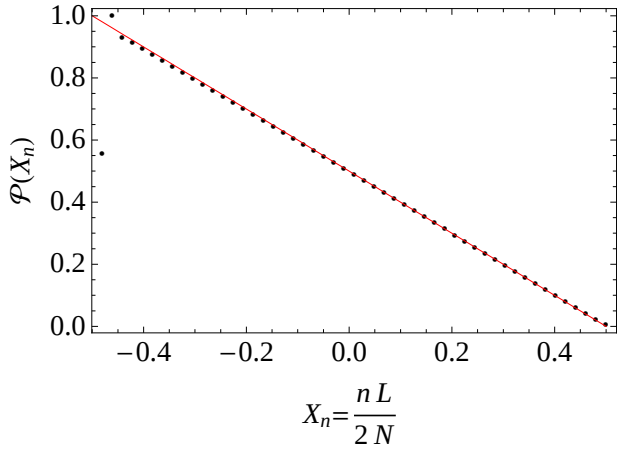

FIG. 2: Non-equilibrium stationary density of the Lorentz channel obtained for a cylinder of length $L = 1$, with 51 disks ($N = 25$). The solid line is $\mathcal{P}(X) = 1/2 - X$, the solution of Eq. (12), with $\mathcal{P}_- = 1$ and $\mathcal{P}_+ = 0$. Notice that the left- and right-most disks are only half disks. Hence the strong boundary effects.

The singular part of the density can also be computed in terms of the statistics of the collision map. For the sake of characterizing this quantity, we notice that the equilibrium Lorentz gas (a single disk on an hexagonal cell with periodic boundary conditions) preserves the Liouville measure

$$\begin{aligned} d\Gamma &= dx\,dy\,dv_x\,dv_y\,, \\ &= dE\,dt\,d\phi\,d\xi, \end{aligned} \tag{14}$$

where ϕ and ξ are the Birkhoff coordinates.

For the open Lorentz gas, we associate to each disk a pair of Birkhoff coordinates, (ϕ_n, ξ_n), and record each collision event in a histogram. The results, displayed in Fig. 3, show the fractality of the fluctuating part of the invariant density, with boundary effects vanishing exponentially fast with respect to the distance of the disk to the channel boundaries.

We will see in Sec. VI that the fractality of the stationary measure displayed in Fig. 3 is responsible for the entropy production rate that is associated to the mass current in the open Lorentz gas with flux boundary conditions.

IV. MULTI-BAKER MAP

The analytic derivation of the entropy production rate (13), relying on the fractality of the invariant measure (10), can be achieved with the multi-baker map. This is a simple model of deterministic diffusion that can be thought of as a caricature of the dynamics of the Lorentz gas described above. This model was originally introduced in [21], its non-equilibrium stationary state and relation to thermodynamics analyzed in [3], and the derivation of the entropy production rate described in [4].

The basic idea which underlies the similarity with the Lorentz channel is threefold. First, let the positions take discrete lattice positions, like the cells $\mathbb{C}_n$ of the channel; second, assume that the collision times τ_n are all identical and denoted by τ, which we leave arbitrary for now; and, third, replace the reflection rules at the collisions by a simple Bernoulli-type angle-doubling rule, which decides which direction the particle goes to. Assuming the system length L to be an integer multiple of the cell size l, which for the sake of the argument we take to be $L = (N+1)l$ with N even, tracer dynamics of the Lorentz channel are replaced by the mapping on $\{-N/2, \ldots, N/2\} \otimes [0, l]^2$, given by

$$B_0 : (n, x, y) \mapsto \begin{cases} (n-1, 2x, y/2)\,, & 0 \le x < l/2\,, \\ (n+1, 2x-l, (y+l)/2)\,, & l/2 \le x < l\,, \end{cases} \tag{15}$$

with the convention that trajectories end when mapped to n outside of $\{-N/2, \ldots, N/2\}$. The map is displayed in Fig. 4. We point out that the multi-baker map has a time-reversal symmetry with respect to the operator $S : (n, x, y) \mapsto (n, l-y, l-x)$, namely $S \circ B_0 = B_0^{-1} \circ S$. The map (15) includes a displacement from cell to cell, which we denote by Λ,

$$\Lambda(n, x, y) \equiv \begin{cases} -l\,, & 0 \le x < l/2\,, \\ +l\,, & l/2 \le x < l\,. \end{cases} \tag{16}$$

Because B_0 is a Bernoulli map, a point $\Gamma = (n, x, y)$ in phase-space may be thought of as coding an infinite sequence of equi-probable nearest-neighbors jumps both in the past and future, with initial condition at position nl. Moreover the variables (x, y), play here the role of the Birkhoff coordinates (ϕ, ξ) of the Lorentz gas.

A. Non-Equilibrium Stationary State

Given flux boundary conditions, a non-equilibrium stationary state similar to that of Eq. (9) sets in, with a singular part given in terms of the sum of the successive displacements the tracer makes before it reaches the outer boundaries and gets absorbed. The x position now becomes a lattice coordinate n and the change in positions between collisions the displacement (16), so that

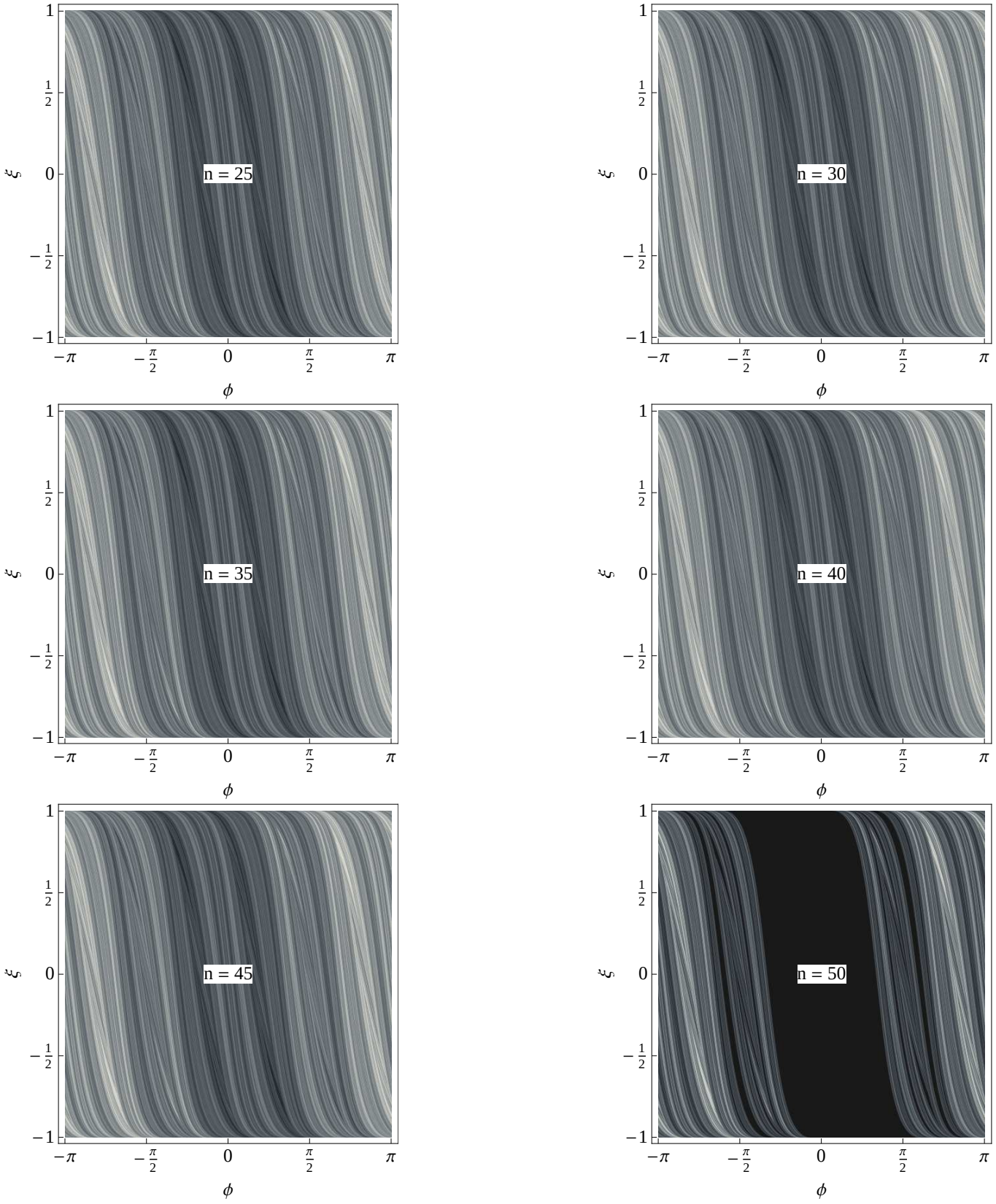

FIG. 3: Fractal structure of the phase portraits of an open cylindrical Lorentz channel with absorbing boundaries at its ends. The plots are histograms computed over grids of 500×500 cells, and counting the average collision rates of many trajectories in every cell. Disk 50 is the one before last. The geometry of the channel is that shown Fig. 1. Here particles are injected at the left boundary only. The color white, associated to higher counting rates, corresponds to the injection of particles from the left boundary. Black areas, on the other hand, correspond to absorption at the right boundary. Hues of gray are associated to phase-space regions whose points are mapped backward to both left and right borders. The corresponding overall densities (11) are shown in Fig. 2.

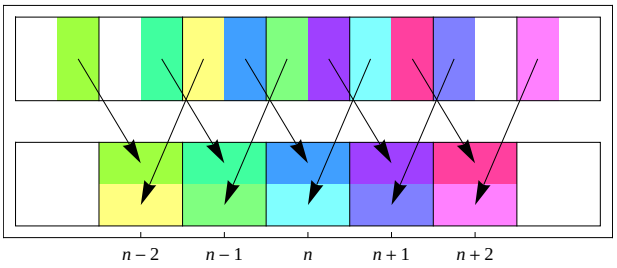

FIG. 4: (Color online) Multi-baker map (15). Each cell has area l^2, with coordinates (x, y), and is labeled by an integer $-N/2 \le n \le N/2$.

the stationary state density reads

$$\rho(\Gamma) = \frac{\rho_+ + \rho_-}{2} + \frac{\rho_+ - \rho_-}{L}\left[n(\Gamma)l + \sum_{k=1}^{K(\Gamma)} \Lambda(B_0^{-k}\Gamma)\right], \tag{17}$$

where $n(\Gamma)$ denotes the projection of Γ along the integer axis.

Since the sum over the successive displacements is a highly singular function of Γ, it is convenient to introduce a better behaved characterization of the invariant density in terms of cumulative functions. Thus let $\Gamma = (n, x, y)$ with $0 \le x, y < l$. We define the set[29]

$$\mathbb{C}_n(x, y) = \{(x', y') \,|\, 0 \le x' < x,\, 0 \le y' < y\}. \tag{18}$$

For $x = y = l$, the cylinder set corresponds to the whole cell, $\mathbb{C}_n \equiv \mathbb{C}_n(l, l)$. The cumulative measure of this set is defined as

$$\begin{aligned} \mu_n(x, y) &= \int_{\mathbb{C}_n(x,y)} d\Gamma \rho(\Gamma)\,, \\ &= \left[\frac{\rho_+ + \rho_-}{2} + (\rho_+ - \rho_-)\frac{nl}{L}\right]\frac{xy}{l^2} \\ &\quad + \frac{\rho_+ - \rho_-}{L}\int_{\mathbb{C}_n(x,y)} d\Gamma \sum_{k=1}^{K(\Gamma)} \Lambda(B_0^{-k}\Gamma)\,. \end{aligned} \tag{19}$$

Here we again assumed normalization of the volume element, $d\Gamma = dx\, dy/l^2$.

It can be shown [3] that the expression above reduces to

$$\mu_n(x, y) = \mu_n \frac{xy}{l^2} + \frac{(\rho_+ - \rho_-)}{L} x T_n\left(\frac{y}{l}\right), \tag{20}$$

where the linear part of the invariant density is

$$\mu_n \equiv \mu_n(l, l) = \frac{1}{2}(\rho_+ + \rho_-) + (\rho_+ - \rho_-)\frac{nl}{L}, \tag{21}$$

and T_n is the incomplete Takagi function [3], which can be defined through the functional equation, here with $y \in [0, 1]$,

$$T_n(y) = \begin{cases} y + \frac{1}{2}T_{n+1}(2y)\,, & 0 \le y < 1/2, \\ 1 - y + \frac{1}{2}T_{n-1}(2y-1)\,, & 1/2 \le y < 1. \end{cases} \tag{22}$$

This equation can be solved recursively using dyadic expansions of x and the boundary conditions $T_{\pm N/2}(x) = 0$. Notice that the size l of the jumps Λ was extracted from the Takagi functions and absorbed into x $(\equiv l \times x/l)$.

We remark that μ_n verifies

$$\mu_n = \frac{1}{2}\mu_{n-1} + \frac{1}{2}\mu_{n+1}, \tag{23}$$

which describes the invariant statistics of a uniform random walk with jump probabilities $1/2$ to nearest neighbors. Given the length l of the jumps, and their rate τ, the diffusion coefficient for this process is $\mathcal{D} = l^2/(2\tau)$. The proper diffusive scaling is recovered provided $\tau \sim l^2$ when $\tau, l \to 0$ in the continuum limit.

In the continuum limit, the number of steps that separate phase points from the boundaries becomes infinite so that the invariant cumulative measure can be written in terms of the (complete) Takagi function,

$$\mu_n(x, y) = \mu_n \frac{xy}{l^2} + \frac{(\rho_+ - \rho_-)}{L} x\, T\left(\frac{y}{l}\right), \quad (N \to \infty)\,. \tag{24}$$

The Takagi function [22], displayed on the top panel of Fig. 5, is the solution of the functional equation

$$T(y) = \begin{cases} y + \frac{1}{2}T(2y)\,, & 0 \le y < 1/2, \\ 1 - y + \frac{1}{2}T(2y-1)\,, & 1/2 \le y < 1. \end{cases} \tag{25}$$

This equation, due to de Rham [23], is one of many equivalent representations of the Takagi function, $T(y) = \sum_{n=0}^{\infty} 2^{-n}\,|2^n y - [2^n y + 1/2]|$, where $[x]$ stands for the maximum integer not exceeding x. It is an everywhere continuous function, but has no bounded derivative.

The singularity of the fluctuating part of the invariant density (17) with respect to the y component can be visualized by measuring the local slopes of the Takagi function. The dependence on the x component on the other hand is trivial. The resulting histogram, displayed on the bottom panel of Fig. 5, can be compared to those shown in Fig. 3 for the Lorentz channel. The main difference is that while the fractal structures are curved in the open Lorentz system, they are parallel to the x-direction in the multi-baker map. The reason is that the fractal structures are smooth with respect to the unstable directions, which, for the multi-baker map, are always directed along the x-axis, while their direction varies from point to point in the Lorentz system.

B. Continuum Limit

As with the Lorentz gas, we let $l \to 0$ and $N \to \infty$, in the continuum limit, keeping $L = (N + 1)l$ constant. In this limit, the macroscopic particle density is to be identified with μ_n, $\mathcal{P}(X_n = nl) = \mu_n$. On the scale of μ_n, the singular fluctuations embodied by the Takagi function disappear. However, as argued in [4], these fluctuations are responsible for the positiveness of the entropy production rate, given according to phenomenology by Eq. (13). We will comeback to this identification in Sec. VI.

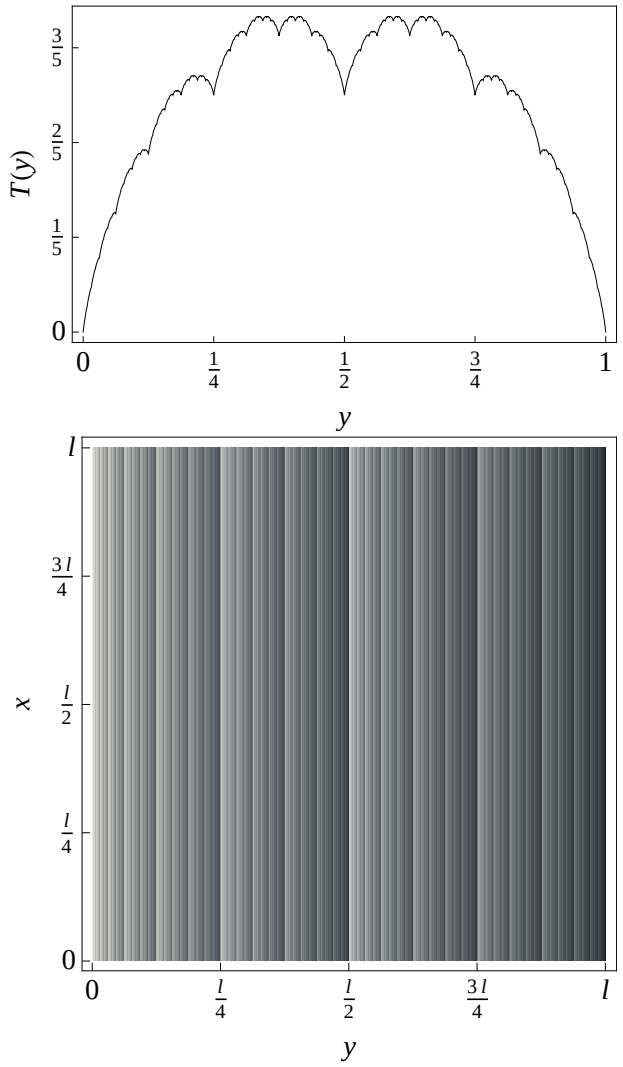

FIG. 5: (Top) The Takagi function, Eq. (25), characterizes the fluctuations of the non-equilibrium stationary state associated to the multi-baker map under flux boundary conditions. (Bottom) The singularity of the invariant density of the multi-baker map (17) can be visualized by measuring the local slopes of the Takagi function (25) at a given scale, here $dy = 1/512$. This histogram can be compared to those obtained for the Lorentz channel, Fig. 3.

V. SPATIALLY PERIODIC SYSTEMS OF INTERACTING PARTICLES

The results presented in Secs. III-IV for diffusive systems of non-interacting tracer particles can be extended to spatially periodic systems of many interacting particles where tagged particles –assumed to be independent of each other– undergo a process of self-diffusion. The arguments below provide an extension to non-equilibrium stationary states of the results presented in [9] for tagged particle diffusion in interacting particle systems undergoing a relaxation to equilibrium.

We follow the diffusion of tracer particles in a periodic array of cells, each containing Q particles, all of them moving with interactions. To this purpose we make the assumption that the density of tracer particles is *dilute*, so that we can consider each tracer particle as though it were the only such particle in each cell at any given time. This is consistent with processes of self-diffusion and mutual diffusion when the tracer is not identical to the other particles. The issue of considering many tagged particles with correlated motions, such as in a process of color diffusion will be discussed in the Conclusions.

Each cell of our system has a finite size domain which is delimited by periodic boundary conditions. This domain can for instance be a square in two dimensions or a cube in three dimensions. The center of mass is taken to be at rest so that no net current takes place. For the sake of the argument, we will assume that the periodic array of cells has a cylindrical structure, extended along one of its spatial dimensions and periodic otherwise.

The dynamics is thus constructed in a way that it is periodic from one cell to the other. A particle entering one cell through any of its borders has a corresponding image which simultaneously leaves that cell through the opposite border, entering the corresponding neighboring cell. The cells located at the boundaries of the array have however a special status since some of their borders are not contiguous to a neighboring cell. Particles can therefore leave the system through these borders, and thus be absorbed, while other particles are correspondingly being injected through the opposite side of the cylinder, entering the corresponding cell through the opposite border. While this process occurs at constant rate, it can nevertheless be used to induce a mass current by simply tagging one of the particles at a time with prescribed rates of injection into the system. This way a molecular dynamics simulation of tracer particle diffusion in a spatially extended system can be set up, which involves a finite number of degrees of freedom only.

Thus consider the cubic box of side l, $\mathbb{I} = [-l/2, l/2]^d \subset \mathbb{R}^d$, containing a collection of Q non-overlapping hard sphere particles of radii σ with phase-space coordinate $\Gamma_Q = \{(\vec{q}_i, \vec{p}_i)\}_{1 \le i \le Q}$, $\vec{q}_i \in \mathbb{I}$, $\vec{p}_i \in \mathbb{R}^d$. Let $\mathbb{C}_n$ denote the phase space of the nth elementary cell. The local dynamics, denoted $\phi^t \Gamma_Q$, preserves the micro-canonical measure and is assumed to be chaotic and mixing.

Given a collection of N copies of such a box, which are placed side by side along the first coordinate axis, the position of a given tracer particle is specified by its coordinate $\vec{q} = (q^1, \ldots, q^d)$ within the elementary box, identical to one out of the Q particles there, and by its lattice position n, $-N/2 \le n \le N/2$ (we assume N even), which distinguishes it from its images in the other lattice cells. Its real coordinate is therefore $(q^1 + nl, \ldots, q^d)$. The flow $\Phi^t\{n, \Gamma_Q\}$ acts over the extended system $\cup_n \mathbb{C}_n$, *i.e.* on the NQ particles of the N elementary cells, out of which a single particle –say the first among Q– has been tagged, the corresponding image being located in cell n, until it moves to a neighboring cell under the time evolution Φ^t . Figure 6 shows an example of such a system

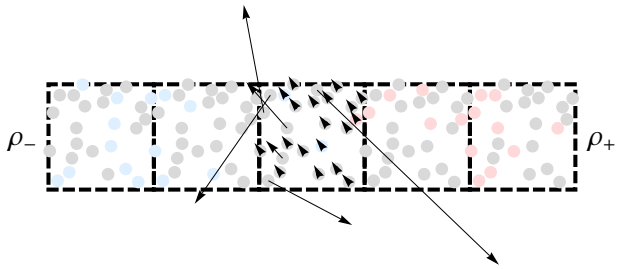

FIG. 6: Example of a spatially periodic system with many interacting particles and one tagged particle in each cell. The tagged particles are randomly injected at the left and right boundaries with suitable probabilities $\rho_\pm$. For purposes of visualization, the number of tracer particles has been exaggerated, mimicking a dilute system where different tracers move independently of one another.

where the number of tracer particles has however been exaggerated for visual purposes. We are indeed assuming a dilute limit according to which no correlations take place between tracer particles.

Given tracer injection rates ρ_- and ρ_+ at the left and right borders, the stationary tracer density is written in a way similar to Eq. (10), in the form

$$\rho(\{n,\Gamma_Q\}) = \frac{\rho_+ + \rho_-}{2} + \frac{\rho_+ - \rho_-}{L}\left\{ L(\{n,\Gamma_Q\}) + \sum_{k=1}^{\infty}\Big[L(\Phi^{-t_k}\{n,\Gamma_Q\}) - L(\Phi^{-t_{k-1}}\{n,\Gamma_Q\})\Big]\right\}. \tag{26}$$

This density is assumed to be normalized with respect to the local micro-canonical distribution of Q particles per cell, and the tracer position along the cylinder axis is $L(\{n,\Gamma_Q\}) = nl + q^1$. We can take the discrete position L instead of the continuous position along the horizontal axis because both give equivalent results since the fractal structures appear through the continuous phase-space dependence of ρ on Γ_Q. The factorization occurs because the tracer dynamics is a simple passive advection process under the assumption that tracer particles do not interact. Thus equilibration of the interacting particles takes place regardless of the tracer dynamics.

The tracer density (26) is a conditional distribution of finding a single tagged particle at the phase point Γ_Q in cell n given the relative injection rates at the system's boundaries. This density is defined with respect to the micro-canonical equilibrium distribution in every cell. The continuum limit is recovered, as with the open Lorentz gas and multi-baker map, by considering an infinite number of copies of independent systems, each with a single tagged particle. The average number of tagged particles as a function of the position along the position coordinate thus yields a macroscopic density which evolves according to the Fokker-Planck equation (3). The tracer dynamics we consider here is therefore much like a single particle system, except for the dimensionality of the phase-space dynamics. In particular the diffusion coefficient depends on the collective motion of the Q interacting particles per periodic cell.

A more physically consistent limit would be to consider the absence of correlations between tracer particles set in motion in the same arbitrary large system. However our formalism for the identification of fractal structures in the non-equilibrium stationary states and the computation of the entropy production rate makes systematic use of the strict spatial periodicity of the dynamics. Its extension to such more general situation requires appropriate elaborations. We leave it as a perspective for the time being.

VI. ENTROPY PRODUCTION

Though a fine-grained Gibbs-type entropy associated to a time-dependent phase-space density $\rho(\Gamma,t)$,

$$S^t(\mathbb{C}_n) = -\int_{\Gamma\in\mathbb{C}_n} d\Gamma\rho(\Gamma,t)[\log\,\rho(\Gamma,t) - 1], \tag{27}$$

is preserved by the time evolution, this is not the case for coarse-grained entropies. This observation has long been understood, see *e.g.* [24, 25], however the novelty here is that, even though the system under consideration is Hamiltonian, the stationary state distribution has a singular density. The fractal structure of the stationary state forbids the use of an entropy like (27). Accordingly, the proper treatment of these phase-space measures requires the use of coarse graining methods.

A systematic approach to defining the proper coarse-grained entropy was outlined in [4, 26]. The idea is that, in the stationary state, owing to the singularity of the invariant density, the Gibbs entropy (27) should

be evaluated by using a grid of phase space, or partition, $\mathbb{G} = \{d\Gamma_j\}$, into small volume elements $d\Gamma_j$, and a time-dependent state $\mu_n(d\Gamma_j, t)$. The entropy associated to cell $\mathbb{C}_n$, coarse grained with respect that grid, is defined according to

$$S^t_{\mathbb{G}}(\mathbb{C}_n) = -\sum_j \mu_n(d\Gamma_j, t) \left[\log \frac{\mu_n(d\Gamma_j, t)}{d\Gamma_j} - 1\right]. \quad (28)$$

This entropy changes in a time interval τ according to

$$\begin{aligned} \Delta^\tau S^t(\mathbb{C}_n) &= S^t_{\mathbb{G}}(\mathbb{C}_n) - S^{t-\tau}_{\mathbb{G}}(\mathbb{C}_n)\,, \quad (29)\\ &= S^t_{\{d\Gamma_j\}}(\mathbb{C}_n) - S^t_{\{\Phi^\tau d\Gamma_j\}}(\Phi^\tau \mathbb{C}_n)\,, \end{aligned}$$

where, in the second line, the collection of partition elements $\{d\Gamma_j\}$ was mapped to $\{\Phi^\tau d\Gamma_j\}$, which forms a partition $\Phi^\tau\mathbb{G}$ whose elements are typically stretched along the unstable foliations and folded along the stable foliations.

Following [9], and in a way analogous to the phenomenological approach to entropy production [10], the rate of entropy change can be further decomposed into entropy flux and production terms according to

$$\Delta^\tau S^t_{\mathbb{G}}(\mathbb{C}_n) = \Delta^\tau_{\rm e} S^t_{\mathbb{G}}(\mathbb{C}_n) + \Delta^\tau_{\rm i} S^t_{\mathbb{G}}(\mathbb{C}_n)\,, \quad (30)$$

where the entropy flux is defined as the difference between the entropy that enters cell $\mathbb{C}_n$ and the entropy that exits that cell,

$$\Delta^\tau_{\rm e} S^t_{\mathbb{G}}(\mathbb{C}_n) = S^t_{\{\Phi^\tau d\Gamma_j\}}(\mathbb{C}_n) - S^t_{\{\Phi^\tau d\Gamma_j\}}(\Phi^\tau \mathbb{C}_n)\,. \quad (31)$$

Collecting Eqs. (29)-(31), the entropy production rate at $\mathbb{C}_n$ measured with respect to the partition $\mathbb{G}$, is identified as

$$\Delta^\tau_{\rm i} S^t_{\mathbb{G}}(\mathbb{C}_n) = S^t_{\{d\Gamma_j\}}(\mathbb{C}_n) - S^t_{\{\Phi^\tau d\Gamma_j\}}(\mathbb{C}_n)\,. \quad (32)$$

This formula is equally valid in the non-equilibrium stationary state.

This *ab initio* derivation of the entropy production rate for non-equilibrium systems with steady mass currents yields results which are in agreement with the phenomenological prescription of thermodynamics. Indeed, as we show below, the entropy production rate of cell $\mathbb{C}_n$, Eq. (32), reduces to the phenomenological entropy production at corresponding position X_n, Eq. (4), as the grid elements become small and the dependence on the choice of partition thus disappears.

A. Multi-baker map

This formalism is particularly transparent for the multi-baker map. Referring to Fig. 4, and having in mind that measures are time-evolved by the inverse map B_0^{-1}, it is easy to see that the bottom horizontal half of cell n is mapped to the left vertical half of cell $n+1$ and, likewise, the top horizontal half of cell n is mapped to the right vertical half of cell $n-1$. Now the invariant measure (24) is uniform with respect to the x coordinate, which is the expanding direction, and has a fractal part along the y axis, the contracting direction. Thus the entropy of the vertical half of cell $n+1$ is half of the entropy of cell $n+1$, but is not equal to the entropy of the bottom or top horizontal halves of that cell, at least not with respect to the same partition.

This observation yields the identification of the entropy production rate, namely the difference between the entropies of that cell, measured at two different levels of resolution, one with respect to volumes $d\Gamma = dxdy$, the other with respect to volumes $d\Gamma' = dx'dy'$, where dy' is twice as large as dy, and dx' half as large as dx.

To be precise, given a resolution level 2^{-k}, $k \in \mathbb{N}$, we consider the collection of cylinder sets $d\Gamma_k(y_j) = \{(x,y)|y_j \le y \le y_j + 2^{-k}l\}$, $j = 1, \ldots, 2^k$, with $y_j = 2^{-k}(j-1)l$, which partition the square into 2^k horizontal slabs of widths $2^{-k}l$, and, by analogy with Eq. (28), define the k-entropy of cell n to be

$$S_k(\mathbb{C}_n) = -\sum_{j=1}^{2^k} \mu_n(d\Gamma_k(y_j)) \left[\log \frac{\mu_n(d\Gamma_k(y_j))}{2^{-k}} - 1\right]. \quad (33)$$

According to Eq. (32), the k-entropy production rate per unit time is

$$\begin{aligned} \Delta^\tau_{\rm i} S_k(\mathbb{C}_n) &= \frac{1}{\tau}\left[S_k(\mathbb{C}_n) - S_{k+1}(\mathbb{C}_n)\right], \quad (34)\\ &= \sum_{j=1}^{2^{k+1}} \mu_n(d\Gamma_{k+1}(y_j)) \log \frac{2\mu_n(d\Gamma_{k+1}(y_j))}{\mu_n(d\Gamma_k(y_{j/2}))}\,, \end{aligned}$$

where the index $j/2$ is the largest integer above $j/2$.

The thermodynamic entropy production rate is recovered in the continuum limit, whereby the local gradients tend to zero and k can be arbitrarily large.

To verify this, we consider the symbolic sequences $\underline{\omega}_k \equiv \{\omega_0, \ldots, \omega_{k-1}\}$, $\omega_j \in \{0,1\}$ associated to the 2^k points y_j through the dyadic expansions $y_j = y(\underline{\omega}_k) = \sum_{j=0}^{k-1} 2^{-j-1}\omega_j$.

In terms of the symbolic sequences $\underline{\omega}_k$, the invariant measure associated to the cylinder set $d\Gamma(\underline{\omega}_k) \equiv d\Gamma(y(\underline{\omega}_k))$ becomes, using Eq. (24),

$$\begin{aligned} \mu_n(\underline{\omega}_k) &= 2^{-k}\mu_n + \nabla\rho\Delta T(\underline{\omega}_k)\,,\\ &= 2^{-k}\mu_n\left[1 + \frac{\nabla\rho}{\mu_n} 2^k \Delta T(\underline{\omega}_k)\right], \quad (35) \end{aligned}$$

where we wrote the local density gradient $\nabla\rho \equiv (\rho_+ - \rho_-)l/L$, and $\Delta T(\underline{\omega}_k) = T\big(y(\underline{\omega}_k)/l + 2^{-k}\big) - T\big(y(\underline{\omega}_k)/l\big)$. Using the functional equation (25), it is straightforward to check that

$$2^k \Delta T(\underline{\omega}_k) = \sum_{j=0}^{k-1} (1 - 2\omega_j)\,, \quad (36)$$

which, up to the scale l, is the displacement associated to points in the cylinder set $d\Gamma(\underline{\omega}_k)$. Two identities are

immediate

$$\begin{array}{l}\sum_{\underline{\omega}_k} 2^k \Delta T(\underline{\omega}_k) = 0, \\ \sum_{\underline{\omega}_k} 2^k \Delta T(\underline{\omega}_k)^2 = k.\end{array} \tag{37}$$

Substituting this expression into Eq. (34), we arrive, after expanding in powers of the density gradient, to the expression

$$\begin{aligned}\Delta_{\rm i}^{\tau} S_k(\mathbb{C}_n) &= \frac{1}{2\tau}\frac{(\nabla\rho)^2}{\mu_n} \\ &\times \left\{ \sum_{\underline{\omega}_{k+1}} 2^{k+1} [\Delta T(\underline{\omega}_{k+1})]^2 - \sum_{\underline{\omega}_k} 2^k [\Delta T(\underline{\omega}_k)]^2 \right\}, \\ &= \frac{1}{2\tau}\frac{(\nabla\rho)^2}{\mu_n} = \frac{l^2}{2\tau L^2}\frac{(\rho_+ - \rho_-)^2}{\mu_n}, \end{aligned} \tag{38}$$

Identifying the diffusion coefficient $\mathcal{D} = l^2 D/\tau$, with $D \equiv 1/2$ the diffusion coefficient associated to the binary random walk, we recover the phenomenological entropy production rate (13) for the macroscopic position variable $X = nl/L$:

$$\lim_{\tau, l \to 0} \Delta_{\rm i}^{\tau} S_k(\mathbb{C}_n) = \frac{d_{\rm i}\mathcal{S}(X_n = nl)}{dt}, \tag{39}$$

where the limit $\tau, l \to 0$ is take with the ration l^2/τ fixed.

B. Lorentz gas

This computation transposes verbatim to the non-equilibrium stationary state of the Lorentz gas, Eq. (10), whose entropy production rate is computed as follows.

Let $\mathbb{M}$ be a partition of $\partial\mathbb{C}$, the phase space of the collision map, into non-overlapping sets A_j, $\mathbb{M} = \cup_j A_j$. We assume that each element of the partition is contained in a cell $\partial\mathbb{C}_n$, *i.e.* $\forall j \, \exists n : A_j \subset \partial\mathbb{C}_n$. There is thus a sub-collection $\mathbb{M}_n$ of cells A_j which partition $\partial\mathbb{C}_n$, $\partial\mathbb{C}_n = \cup_{j\,:\,A_j \in \mathbb{M}_n} A_j$. Moreover we assume all the partitions $\mathbb{M}_n$ are isomorphic, which is to say they can be obtained from one another by translation.

We construct such a partition of the phase space associated to cell n by dividing up $\partial\mathbb{C}_n$ into sets A_j according to the displacements of points $\Gamma \in A_j$, such as shown in Fig. 7. Thus a k partition $\mathbb{M}_n^k$ of $\mathbb{C}_n$ is a collection of sets $A(\omega_0, \ldots, \omega_{k-1})$ of points Γ which have coherent horizontal displacements for the first k steps. These displacements are coded by sequences of symbols $\underline{\omega}_k$ which, in this case, take at most 12 possible values, corresponding to the twelve possible transitions to the nearest and next-nearest neighboring disks. However, unlike with Bernoulli processes, not all symbol sequences are allowed so that the number of sets in the partition $\mathbb{M}_n^k$ is much less than 12^k. This is referred to as pruning [27, 28].

Assuming $\omega_j \in \{1, \ldots, 12\}$, we define $a(\omega_j)$ as the displacement along the horizontal axis corresponding to the label ω_j, and

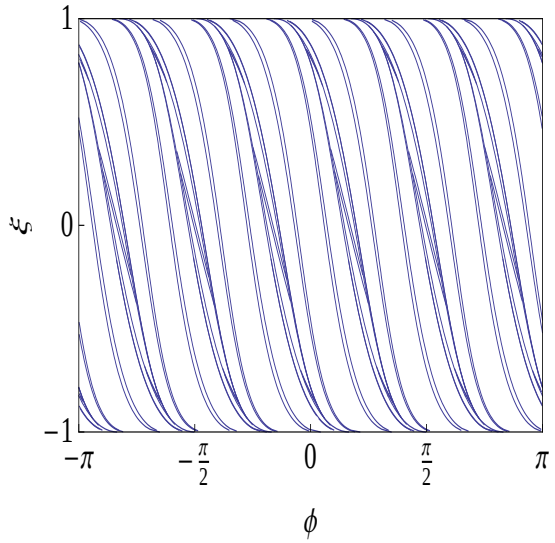

FIG. 7: The partition of a unit cell of the open periodic Lorentz gas constructed upon two iterations of the collision map. The borders of the elements of the partition are the lines of discontinuity of the collision map in the (ϕ, ξ) plane. Each point of the curves belongs to a trajectory that grazes a disk in one or two iterates.

$$\delta(\underline{\omega}_k) \equiv \sum_{j=0}^{k-1} a(\omega_j), \tag{40}$$

which, up to the local length scale l, is the displacement associated to the sequence $\underline{\omega}_k$, measured with respect to the position of the scatterers.

The measure associated to these sets is defined by

$$\mu(\underline{\omega}_k) = \int_{A(\underline{\omega}_k)} d\Gamma \rho(\Gamma), \tag{41}$$

where ρ is the invariant density associated to the flux boundary conditions, Eq. (10). Inserting this expression into Eq. (41), we may write

$$\begin{aligned}\mu(\underline{\omega}_k) &= \mu_n \nu(\underline{\omega}_k) \\ &+ \frac{\rho_+ - \rho_-}{L} \int_{A(\underline{\omega}_k)} d\Gamma \sum_{k=1}^{\infty} [x(\Phi^{-t_k}\Gamma) - x(\Phi^{-t_{k-1}}\Gamma)], \end{aligned} \tag{42}$$

where

$$\mu_n = \frac{\rho_+ + \rho_-}{2} + (\rho_+ - \rho_-)\frac{nl}{L}, \tag{43}$$

and $\nu(\underline{\omega}_k) = \int_{A(\underline{\omega}_k)} d\Gamma$ is the volume measure associated to the set $A(\underline{\omega}_k)$, with $\nu(\underline{\omega}_k) = 0$ whenever $\underline{\omega}_k$ is a pruned sequence.

We claim that we can make the approximation

$$\begin{aligned}\frac{1}{\nu(\underline{\omega}_k)} \int_{A(\underline{\omega}_k)} d\Gamma \frac{1}{l} \sum_{j=1}^{\infty} \Big[x(\Phi^{-t_j}\Gamma) \; - \; x(\Phi^{-t_{j-1}}\Gamma) \Big] \\ \simeq \; \delta(\underline{\omega}_k), \end{aligned} \tag{44}$$

which we expect to hold provided k is large. This quantity therefore plays, for the non-equilibrium stationary state of the Lorentz gas, a role similar to that played under the same conditions by $\Delta T(\underline{\omega}_k)/\nu(\underline{\omega}_k)$, Eq. (36), for the multi-baker map. Indeed the difference between the two sides of Eq. (44) is $\mathcal{O}(1)$. Under this condition and assuming $l \ll 1$, we thus write

$$\mu(\underline{\omega}_k) = \nu(\underline{\omega}_k)\mu_n \left[1 + \frac{\rho_+ - \rho_-}{\mu_n}\frac{l}{L}\delta(\underline{\omega}_k)\right] , \qquad (45)$$

which can be compared to Eq. (35). When k is large, identities similar to Eq. (37) hold for $\delta(\underline{\omega}_k)$:

$$\begin{array}{l} \sum_{\underline{\omega}_k} \nu(\underline{\omega}_k)\delta(\underline{\omega}_k) = 0 \, , \\ \sum_{\underline{\omega}_k} \nu(\underline{\omega}_k)\delta(\underline{\omega}_k)^2 = 2Dk \, , \end{array} \qquad (46)$$

where the diffusion coefficient D is that of the random walk on half integer lattice sites associated to the displacements (40) with weights $\nu(\underline{\omega}_k)$.

The computation of the entropy production rate (32) then proceeds along the lines of Eq. (38), with a similar result:

$$\Delta_{\rm i}^{\tau} S_k(\mathbb{C}_n) = \frac{l^2 D}{\tau L^2}\frac{(\rho_+ - \rho_-)}{\mu_n} , \qquad (47)$$

in agreement with the phenomenological expression Eq. (13) with diffusion coefficient $\mathcal{D} = l^2 D/\tau$ and position $X_n = nl/2$.

C. Interacting particle system

Here, as in Ref. [9], we assume a partition of phase-space in sets A_j sufficiently small that all points in them have particle No. 1 flowing through the same sequence of cells over a large time interval, *i.e.* such that the set of points $\Phi^{-\tau}A_j$ are in the same cell when projected along the coordinate of particle No. 1, with $0 \leq \tau \leq \mathcal{T}$. The corresponding location is $L(\Phi^{-\tau}\{n, \Gamma_Q\})$, $\Gamma_Q \in A_j$. We define the displacement

$$\mathrm{d}(\Gamma_Q, t) = L(\Phi^{-t}\{n, \Gamma_Q\}) - nl \, , \qquad (48)$$

and write the non-equilibrium stationary state as

$$\mu(A_j) = \mu_n \nu(A_j) + \frac{\rho_+ - \rho_-}{L}\int_{A_j} d\Gamma_Q \mathrm{d}(\Gamma_Q, \mathcal{T}) \, , \qquad (49)$$

where the volume measure $\nu(A_j)$ is the micro-canonical measure of the periodic system of Q particles. The integral in this expression encodes the fluctuating part of the non-equilibrium stationary state. In analogy to Eq. (44), we can write

$$\delta(A_j) = \frac{1}{\nu(A_j)}\int_{A_j} d\Gamma_Q \mathrm{d}(\Gamma_Q, \mathcal{T}) \, , \qquad (50)$$

in terms of which we have the identities

$$\begin{array}{l} \sum_j \nu(A_j)\delta(A_j) = 0 \, , \\ \sum_j \nu(A_j)\delta(A_j)^2 = 2\mathcal{D}\mathcal{T} \, , \end{array} \qquad (51)$$

which, apart for their dimensions, are similar to Eqs. (37) and (46).

Proceeding as with the multi-baker map and Lorentz gas, we have the entropy production rate

$$\Delta_{\rm i}^{\tau} S_{\mathcal{T}}(\mathbb{C}_n) = \frac{\mathcal{D}}{L^2}\frac{(\rho_+ - \rho_-)}{\mu_n} , \qquad (52)$$

independently of the resolution scale set by the time parameter $\mathcal{T}$.

VII. CONCLUSION

In this paper we have considered a large class of diffusive deterministic systems with volume-preserving dynamics, and established the fractality of the non-equilibrium stationary states which result from the stochastic injection of particles at the systems' boundaries.

Under the assumption that the dynamics is chaotic, the natural non-equilibrium invariant measure is characterized by a phase-space density which is the stationary state of a Liouville or Perron-Frobenius operator with flux boundary conditions, which account for the presence of particle reservoirs. This density naturally splits into regular and singular parts. The regular part has a local equilibrium form, uniform with respect to the scale of macroscopic variables. It is the natural counterpart on phase space of the solution of the macroscopic transport equation under non-equilibrium boundary conditions, displaying a linear density gradient. In contrast, the singular part varies non-continuously on microscopic scales, reflecting the sensitive dependence on initial conditions, and has no macroscopic counterpart.

The fundamental achievement of this paper is to have exhibited the universal features of the non-equilibrium stationary states of simple low-dimensional deterministic models of diffusion, which are shared by higher dimensional spatially periodic systems modeling tagged particle diffusion. As already pointed out in [18], the fractality of the non-equilibrium stationary states is the key to a systematic computation of the positive entropy production rate. Indeed the fractality of phase-space distributions imposes the use of coarse-graining techniques in order to define the entropy. The coarse-graining of phase-space into partitions of sets of strictly positive volumes results into an entropy which is generally not constant in time. The decomposition of the time evolution of such coarse-grained entropies into entropy flux and entropy production terms provides a framework in which the positiveness of the entropy production rate can be rigorously established. Furthermore, in the macroscopic limit, two key results are obtained: (i) the entropy production rate is independent of the coarse graining in the limit of arbitrarily fine phase-space graining, and (ii) its value is identical to the phenomenological rate of entropy production, according to thermodynamics.

In this respect, this paper helps clarify a point that had been overlooked in previous works. Under the diffusive scaling limit, the local particle density gradient is a natural small parameter in the continuous limit: fixing the injection rates and system size, we let the spacing between cells go to zero in order to obtain the macroscopic limit. With the identification of this small parameter, it is straightforward to verify that the computation of the entropy production of the non-equilibrium stationary states, whether of multi-baker maps, Lorentz gases, or spatially periodic systems, all yield leading contributions consistent with the prescription of thermodynamics.

As we have pointed out, the formalism we use relies systematically on the spatial periodicity of the dynamics, especially with regards to identifying the rate of entropy production. Though this periodicity is convenient as it enables one to clearly identify a separation of scales between microscopic and macroscopic motions, it is a rather restrictive and ultimately undesirable feature of our models. One would rather describe the diffusive motion of dilute tracer particles in arbitrary systems. It is our hope that this work helps set the stage to achieve this more ambitious goal in future works.

As mentioned in the introduction, this paper is the first of two. In the companion paper [12], we consider the influence of an external field on spatially periodic diffusive volume-preserving systems, *i.e.* forced systems in which no dissipative mechanism is present. As proved by Chernov and Dolgopyat [15], such systems are recurrent in the sense that tracer particles keep coming back to the region of near zero velocity where all the energy is transferred into potential energy, so that no net current takes place. We show that these systems remain diffusive, albeit with a velocity-dependent diffusion coefficient which alters the usual scaling laws and consider their statistical properties in some details.

Acknowledgments

This research is financially supported by the Belgian Federal Government (IAP project "NOSY") and the "Communauté française de Belgique" (contract "Actions de Recherche Concertées" No. 04/09-312) as well as by the Chilean Fondecyt under International Cooperation Project 7070289. TG is financially supported by the Fonds de la Recherche Scientifique F.R.S.-FNRS. FB acknowledges financial support from the Fondecyt Project 1060820 and FONDAP 11980002 and Anillo ACT 15.

[1] J. W. Gibbs, *Elementary Principles in Statistical Mechanics*, (Yale U. Press, New Haven, 1902); reprinted (Dover Publ. Co, New York, 1960).

[2] I. Cornfeld, S. Fomin and Ya. Sinai, *Ergodic Theory*, (Springer-Verlag, New York, 1982).

[3] S. Tasaki and P. Gaspard, *Fick's law and fractality of nonequilibrium stationary states in a reversible multibaker map*, J. Stat. Phys. **81** 935 (1995).

[4] P. Gaspard, *Entropy production in open volume-preserving systems*, J. Stat. Phys. **88** 1215 (1997).

[5] S. Tasaki and P. Gaspard, *Thermodynamic behavior of an area-preserving multibaker map with energy*, Theor. Chem. Acc. **102** 385 (1999).

[6] S. Tasaki and P. Gaspard, *Entropy Production and Transports in a Conservative Multibaker Map with Energy*, J. Stat. Phys. **101** 125 (2000).

[7] T. Gilbert and J. R. Dorfman, *Entropy Production in a Persistent Random Walk*, Physica A **282** 427 (2000).

[8] T. Gilbert, J. R. Dorfman and P. Gaspard, *Entropy Production, Fractals, and Relaxation to Equilibrium*, Phys. Rev. Lett. **85** 1606 (2000).

[9] J. R. Dorfman, P. Gaspard and T. Gilbert, *Entropy production of diffusion in spatially periodic deterministic systems*, Phys. Rev. E **66** 026110 (2002).

[10] S. de Groot and P. Mazur, *Non-equilibrium Thermodynamics*, (North-Holland, Amsterdam, 1962); reprinted (Dover Publ. Co., New York, 1984).

[11] P. Gaspard, *Chaos, Scattering, and Statistical Mechanics*, (Cambridge University Press, Cambridge UK, 1998).

[12] F. Barra, P. Gaspard and T. Gilbert, *Fractality of the non-equilibrium stationary states of open volume-preserving systems: II. Galton boards*, preprint (2009).

[13] F. Galton, *Natural inheritance*, (Macmillan, 1889).

[14] M. Barile and E. W. Weisstein, *Galton Board*, From MathWorld–A Wolfram Web Resource. http://mathworld.wolfram.com/GaltonBoard.html

[15] N. Chernov and D. Dolgopyat, *Diffusive motion and recurrence on an idealized Galton board*, Phys. Rev. Lett. **99** 030601 (2007).

[16] N. Chernov and D. Dolgopyat, *Galton Board: limit theorems and recurrence*, preprint (2007).

[17] P. Gaspard, G. Nicolis and J. R. Dorfman, *Diffusive Lorentz gases and multibaker maps are compatible with irreversible dynamics*, Physica A **323** 294-322 (2003).

[18] P. Gaspard, *Chaos and hydrodynamics*, Physica A **240** 54 (1997).

[19] J. L. Lebowitz, *Stationary Nonequilibrium Gibbsian Ensembles*, Phys. Rev. **114** 1192 (1959).

[20] J. A. McLennan, *Statistical Mechanics of the Steady State*, Phys. Rev. **115** 1405 (1959).

[21] P. Gaspard, *Diffusion, effusion, and chaotic scattering: An exactly solvable Liouvillian dynamics*, J. Stat. Phys. **68** 673 (1992).

[22] T. Takagi, *A simple example of continuous function without derivative*, Proc. Phy.-Math. Soc. Japan **1** 176 (1903).

[23] G. de Rham, *Sur un exemple de fonction continue sans dérivée*, Enseign. Math. **3**, 71 (1957); *Sur quelques courbes définies par des équations fonctionnelles* Rend. Sem. Mat. Torino **16**, 101 (1957).

[24] R. C. Tolman, *The Principles of Statistical Mechanics*, (Oxford, London, 1938); reprinted (Dover Publications, New York, 1979).

[25] P. and T. Ehrenfest, *The Conceptual Foundations of the Statistical Approach in Mechanics*, (Cornell University

Press, Ithaca, 1959); reprinted (Dover Publications, New York, 2002).

[26] T. Gilbert and J. R. Dorfman, *Entropy Production : From Open Volume Preserving to Dissipative Systems*, J. Stat. Phys. **96** 225 (1999).

[27] P. Cvitanović, P. Gaspard, and T. Schreiber, *Investigation of the Lorentz gas in terms of periodic orbits*, Chaos **2** 85 (1992).

[28] P. Cvitanović, J.-P. Eckmann, and P. Gaspard, *Transport properties of the Lorentz gas in terms of periodic orbits*, Chaos, Solitons and Fractals **6** 113 (1995).

[29] Such sets are usually referred to in the literature as cylinder sets.